Published in IEEE Transactions on Ultrasonics, Ferroelectrics, and Frequency Control 67, issue 1, 207-2016, 2020
which should be used for any reference to this work

Long-Term Stability Analysis Toward $<10^{-14}$ Level for a Highly Compact POP Rb Cell Atomic Clock

Nil Almat, Mohammadreza Gharavipour, William Moreno, Florian Gruet, Christoph Affolderbach, *Member, IEEE*, and Gaetano Mileti, *Member, IEEE*

***Abstract*— Long-term frequency instabilities in vapor-cell clocks mainly arise from fluctuations of the experimental and environmental parameters that are converted to clock frequency fluctuations via various physical processes. Here, we discuss the frequency sensitivities and the resulting stability limitations at one-day timescale for a rubidium vapor-cell clock based on a compact magnetron-type cavity operated in air (no vacuum environment). Under ambient laboratory conditions, the external atmospheric pressure fluctuations may dominantly limit the clock stability via the barometric effect. We establish a complete long-term instability budget for our clock operated under stable pressure conditions. Where possible, the fluctuations of experimental parameters are measured via the atomic response. The measured clock instability of $<2 \times 10^{-14}$ at one day is limited by the intensity light-shift effect, which could further be reduced by active stabilization of the laser intensity or stronger optical pumping. The analyses reported here show the way toward simple, compact, and low-power vapor-cell atomic clocks with excellent long-term stabilities $\leq 10^{-14}$ at one day when operated in ambient laboratory conditions.**

***Index Terms*— Atomic clocks, frequency shifts, metrology, Ramsey scheme, rubidium, stability analysis, vapor cells.**

I. Introduction

COMPACT vapor-cell atomic clocks play a crucial role in many applications based on high-precision timing, such as satellite-based navigation and positioning systems [1], and synchronization in communications [2], [3] and power grids [4], [5]. The main characteristics of such clocks are small volume and low power consumption, along with excellent short- and long-term frequency stability. In particular, satellite-based navigation systems require excellent long-term frequency stabilities at the level of $<10^{-14}$ at one day.

Manuscript received June 29, 2019; accepted September 8, 2019. This work was supported in part by the Swiss National Science Foundation (SNSF) under Grant 156621, in part by the European Union's Horizon 2020 Research and Innovation Program through Quantum Technology Flagship, Project macQsimal under Grant 820393, in part by the European Space Agency (ESA), and in part by the EMRP Project IND55-Mclocks. *(Corresponding author: Nil Almat.)*

N. Almat, F. Gruet, C. Affolderbach, and G. Mileti are with the Laboratoire Temps-Fréquence, Institut de Physique, Université de Neuchâtel, 2000 Neuchâtel, Switzerland (e-mail: nil.almat@unine.ch; gaetano.mileti@unine.ch).

M. Gharavipour was with the Laboratoire Temps–Fréquence, Université de Neuchâtel, Switzerland. He is now with TRUMPF Photonic Components, 89081 Ulm, Germany.

W. Moreno was with the Laboratoire Temps-Fréquence, Université de Neuchâtel, Switzerland. He is now with the Laboratoire national de métrologie et d'essais, Système de Références Temps-Espace, 75014 Paris, France.

Various clock operating approaches are exploited in different laboratories to reach such stability performances. The continuous-wave (CW) double-resonance (CW-DR) scheme based on two simultaneous interaction fields (optical and microwave) applied on the vapor cell has demonstrated excellent short-term stabilities [6], with the long-term stability limited mainly by light-shift effects [7], [8]. The pulsed optically pumped (POP) interrogation scheme separates the optical and microwave interrogation in the time domain and has experimentally demonstrated reduced light-induced instability contributions [9]–[12]. Also, for the alternative coherent population trapping (CPT) [13] approach, similar methods were proposed to reduce clock instabilities due to the light-shift effects [14], [15]. In addition to such light-induced effects, several other experimental and environmental parameters may significantly limit the measured clock instability [16].

The long-term instability budget of a vapor-cell POP Rb clock based on the maser signal detection (free induction decay of the atoms after microwave interrogation) was covered in [17]. The physics package (PP) understudy in [17] includes a microwave cavity with a high-quality factor ($Q \approx 10\,000$) placed in vacuum. Such high-Q of the cavity is crucial for clock signal detection in the microwave domain, but can seriously limit the clock stability through the cavity-pulling effect [18], which, in this case, presents the dominant instability source arising from fluctuations in microwave power and external pressure. Placing the PP under vacuum drastically reduces pressure fluctuations on the PP and the related cavity-pulling instabilities [17], but makes the system bulky and power consuming in some applications.

In the following, we present a detailed analysis and budget of the long-term instability for a highly compact rubidium vapor-cell clock, based on our preliminary analysis reported in [19]. The clock employs a time-domain Ramsey interrogation with laser optical detection. It operates under ambient laboratory conditions, which can notably simplify the clock system and reduce its size, weight, and power consumption. Optical detection of the clock signal allows using a low-Q ($\approx$140) microwave cavity; hence, reduces contribution of the cavity-pulling effect and enables a highly compact cavity design [20]. For this clock prototype, we have previously demonstrated short-term stability of 2.1×10^{-13} at 1 s averaging time, limited by the signal-to-noise ratio (SNR) of the optically detected signal [10], and reduced light-shift instability contributions [21]. Then, we have reported

on the numerical studies conducted on the origin of the microwave power sensitivities in our clock [22]. The interplay of the inhomogeneity in the microwave field amplitude in the cavity with an inhomogeneous light-shift distribution along the cell was identified as the main contributor, whereas the contribution of the cavity-pulling effect remains negligible. We have also shown that in ambient laboratory conditions, the dominant contribution to clock instability may arise from ambient pressure fluctuations via the barometric effect [23]. A preliminary analysis of instability sources toward a complete long-term budget was presented in [19]. Here, we evaluate in detail the clock sensitivities to experimental and environmental parameter fluctuations and quantify the resulting clock stability limits on long-term timescales up to one day.

In the next sections, we first describe the clock prototype used in this work. Then, we give the long-term instability budget for our clock prototype, including all known physical effects relevant on timescales from 10^4 up to 10^5 s (one day) of averaging time. The clock frequency sensitivities discussed here present an extensive list of instability sources to be taken into consideration for the realization and enhancement of compact vapor-cell clocks toward excellent long-term stabilities ($<10^{-14}$ at one day), in the laboratory or commercial prototypes for ground-based, as well as space-borne applications. While we report on the long-term stability limits for our POP Rb vapor-cell clock, many relevant physical processes are similar for vapor-cell clocks operated with other interrogation schemes (CW-DR, CPT, Ramsey-CPT, etc.)

II. Experimental Apparatus

The basic scheme for the Rb vapor-cell clock setup shown in Fig. 1(a) is composed of three main blocks [21]: 1) an *optical source* for pulsed laser light; 2) the *physics package*, including the Rb vapor cell and microwave cavity; and (3) the *electronics* [24] for generating the microwave field interrogating the atoms and its frequency stabilization loop. The clock's pulse sequence, as illustrated in Fig. 1(b), comprises an intense light pulse for the optical pumping during $T_p = 0.4$ ms, two microwave pulses of duration $T_m = 0.3$ ms each, separated by the Ramsey-free evolution time of $T_{\text{Ramsey}} = 3$ ms, and a weak light pulse for optical detection for $T_d = 0.7$ ms.

First, the compact *optical source* [25] is based on a distributed feedback (DFB) laser generating 780-nm light (^{87}Rb D_2 line). The choice of the D_2 line is mainly based on the availability of the compact DFB laser diodes with suitable spectral properties, as well as the enhanced short-term clock instability compared to the use of the D_1 line [26]. The laser frequency is stabilized to a sub-Doppler peak of a (direct or crossover) transition from the $|5^2S_{1/2}, F = 2\rangle$ ground state, obtained from a separate evacuated Rb cell [see Fig. 1(c)]. The optical pulses are realized via an acousto-optic modulator (AOM) exhibiting rise and fall switching times of 4.5 μs. The optical power during the pumping and detection phases is 14 and 150 μW, respectively, and the residual light during the Ramsey time is measured at the level of 0.2 μW at the PP input, corresponding to a 48-dB extinction ratio with respect to the optical pump power. The beam diameter in the clock cell

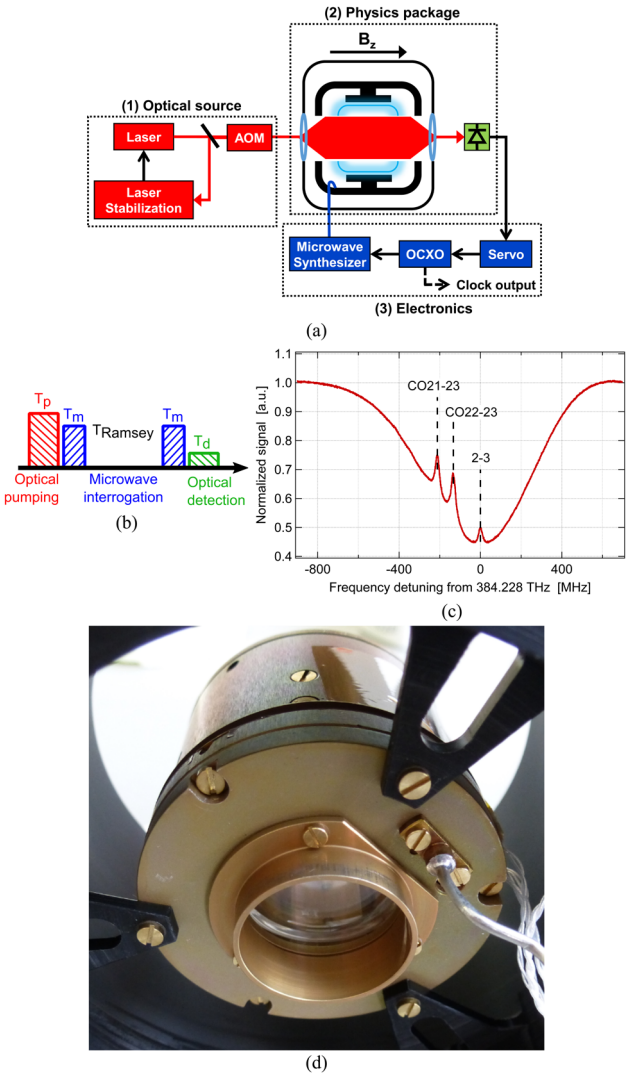

Fig. 1. (a) Schema of the Rb vapor-cell clock setup. (b) Pulse sequence of the time-domain Ramsey scheme applied to the vapor cell. (c) The sub-Doppler absorption spectrum of the $|5^2S_{1/2}, F = 2\rangle$ ground state, detected in a separate evacuated Rb cell used for laser frequency stabilization. (d) Photograph of the compact magnetron cavity under assembly, outer cavity diameter is 43 mm.

is ~19 mm. Currently, no active light-intensity stabilization is applied.

Second, the *physics package* holds the vapor cell (25-mm diameter and length) which contains the Rb atoms and the buffer gases (argon and nitrogen) and is temperature-stabilized at the inversion temperature of 62.16 °C for the used buffer-gas mixture (see Section III-E). A stem on the cell, serving as a reservoir for Rb atoms, is kept at 59 °C. The vapor cell is held by a compact magnetron-type microwave cavity of 45 cm^3 volume, see Fig. 1(d) [20] whose resonance frequency coincides with the Rb ground-state hyperfine splitting frequency ($\nu_{\text{Rb}} = 6\,834\,682\,611$ Hz) to 1.9 MHz. The relatively low Q-factor ($Q \approx 140$) of the cavity (resonance linewidth of ~50 MHz) avoids issues arising from long-term frequency drifts of the resonance frequency observed for high-Q cavities [17]. A solenoid carrying a stabilized direct

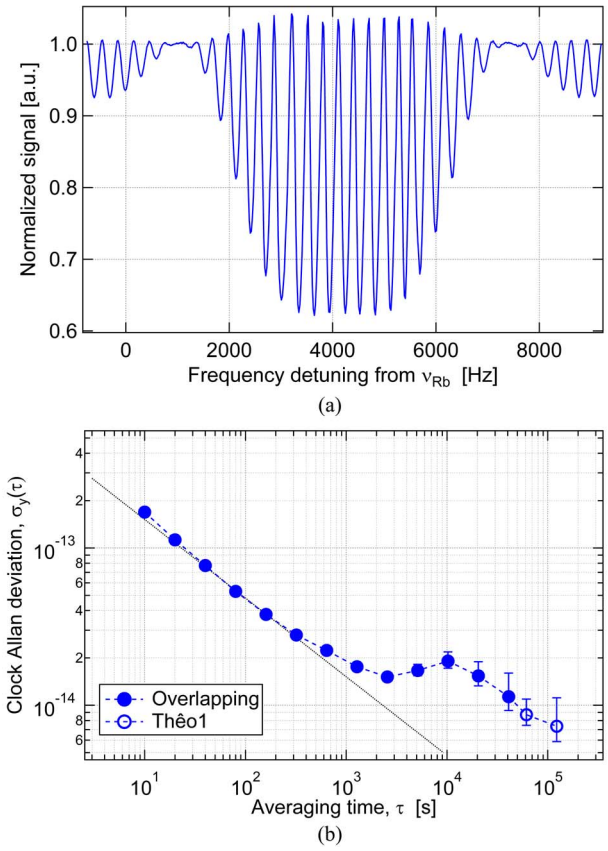

Fig. 2. (a) Ramsey pattern observed under typical clock operating conditions described in Section II with optical pump and detection frequencies tuned on CO21-23 and microwave pulse areas $\theta = 0.56 \cdot \pi$. (b) Clock frequency instability measurement of 3 days. No drift removal was undertaken.

current generates a static magnetic field (C-field) of 3.5 μT across the vapor cell, thus defining the quantization axis and allowing to access the $|5^2S_{1/2}, F = 1, m_F = 0\rangle \rightarrow |5^2S_{1/2}, F = 2, m_F = 0\rangle$ clock transition. The PP assembly is placed in the thermal isolation and two-layer mu-metal shield.

Third, the *electronics* part generates the microwave signal applied to the atoms, based on frequency multiplication from a quartz oscillator (OCXO) [24]. It also controls the time synchronization of the optical and microwave pulses and generates the error signal by synchronous demodulation of the optically detected atomic response. The clock operates at a microwave pulse area slightly higher than the conventional $\pi/2$ pulses employed in [21] (see Section III-B). This reduces the clock sensitivity to microwave power fluctuations by one order of magnitude [27]. The clock instability is measured as the 10-MHz output of the stabilized quartz local oscillator against a hydrogen maser referenced to GPS.

A typical Ramsey clock signal is shown in Fig. 2(a) and has ~40% contrast and a central fringe linewidth of 160 Hz. The typical frequency instability of our clock prototype is reported in Fig. 2(b). A single data set was analyzed using the ThêoH deviation, which is based on the overlapping Allan deviation in the short term and Thêo1 deviation in the long term allowing to extend the statistical analysis in longer timescales than the Allan deviation and with better confidence levels. This data is measured in ambient laboratory conditions, with only the PP placed in a hermetic chamber to reduce the impact of atmospheric pressure fluctuations (see Section III-A). The measured short-term clock instability of $4.8 \times 10^{-13}\ \tau^{-1/2}$ is principally limited by the optical detection noise, which is degraded by about a factor of 2 since our previously reported short-term performance in [10] resulting, mainly, from the implementation of the more compact laser optical source [25]. The long-term clock stability reaches $<2 \times 10^{-14}$ for 10^4–10^5 s averaging times, mainly limited by the light intensity fluctuations (see Section III-C). The different contributions to the measured long-term frequency instability of our clock are discussed in the next sections.

III. Long-Term Instability Sources

The vapor-cell clock frequency is sensitive to fluctuations of the experimental and environmental parameters [16] via different physical processes [7] characterized by their related sensitivity coefficients. In this section, we evaluate all the important physical effects that affect our clock's stability performance on long-term timescales and discuss the resulting clock stability limitations.

A. Barometric Effect

Environmental pressure fluctuations can impact the clock frequency by different means [16], [28]–[30]. In the case of our clock setup, the dominant contribution is the so-called barometric effect due to the variation of the buffer-gas pressure in the cell induced by the bending of the cell windows in response to varying external pressure [23].

Typical atmospheric pressure fluctuations can reach 3 hPa (in terms of Allan deviation) at one-day timescale and result in a clock instability contribution at the level of 10^{-13}. For reducing the impact of the barometric effect on a clock operated in ambient laboratory conditions, various solutions may be adopted [23]. For a first demonstration, we employ here a hermetic chamber to realize an environment of stable external pressure for the PP. The internal temperature of the chamber (measured on top of the PP) is controlled via an actively stabilized baseplate temperature in the short term, yet in the long-term timescales, it is governed by the residual external temperature fluctuations transferred through the walls and windows, and by the air inside the chamber. The pressure fluctuations in the chamber are at the level of 0.03 hPa over one day, limited by the internal temperature fluctuations via the ideal gas law. The environmental and chamber pressure and temperature fluctuations measured simultaneously are shown in Fig. 3. The external pressure fluctuations are eliminated in the PP environment, and those of the temperature are reduced. The temperature sensitivities of our clock are at a negligible level (see Section III-E); thus, a small reduction of the pressure is sufficient to keep the clock instability contribution due to the barometric sensitivities below 10^{-14}.

The clock frequency sensitivity to the chamber pressure measured under low-pressure conditions (535 hPa) is $(6.6 \pm 0.2) \times 10^{-14}$ /hPa, in agreement with previously reported data [23], [27]. The pressure fluctuations inside the chamber lead

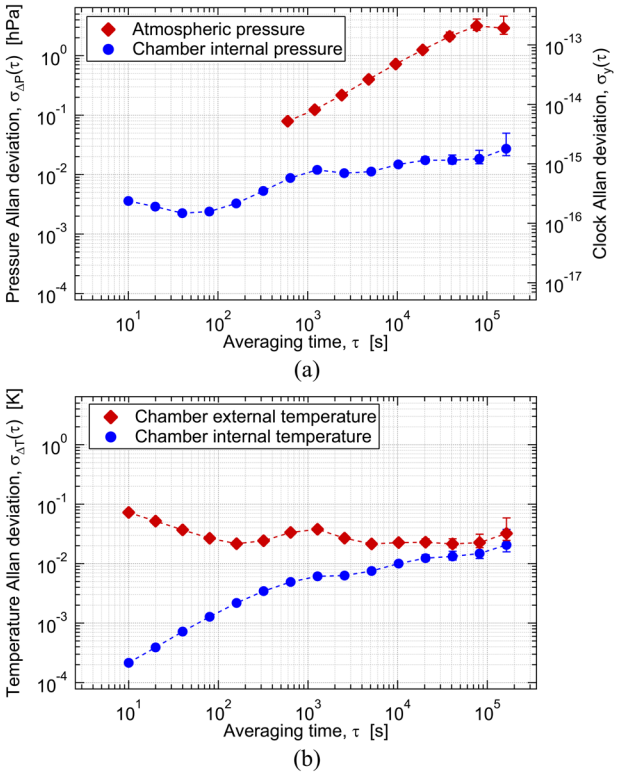

Fig. 3. (a) Environmental (diamonds) and chamber (rounds) pressure fluctuations measured simultaneously. Left axis: in terms of pressure fluctuations. Right axis: in terms of relative clock frequency fluctuations. (b) Laboratory (diamonds) and chamber (rounds) temperature fluctuations measured simultaneously with the data in (a). Environmental pressure data is provided by MeteoSwiss.

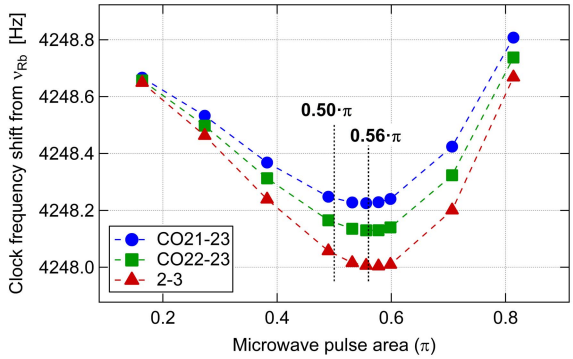

Fig. 4. Clock frequency shift as a function of the normalized microwave pulse area $\theta = b \cdot T_m$ for laser frequencies labeled, as shown in Fig. 1(c).

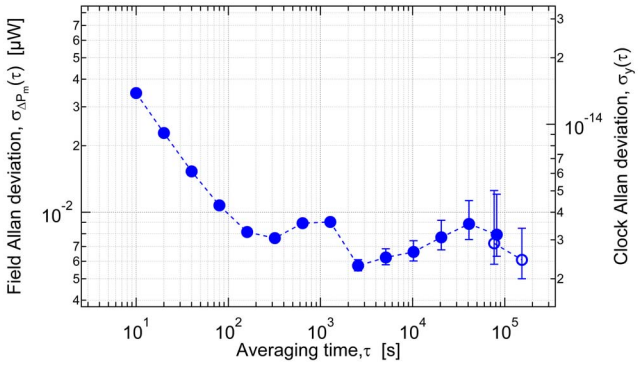

Fig. 5. Microwave power fluctuations. Left axis: in terms of microwave power injected in the cavity. Right axis: in terms of relative clock frequency fluctuations for operation at $\theta = 0.56 \cdot \pi$.

to a clock instability contribution due to the barometric effect reduced to 2×10^{-15} at one day, allowing the analysis of other clock instability contributions at the level of 10^{-14}. The absolute clock frequency shift when passing from atmospheric pressure (∼970 hPa) to 535 hPa is estimated at −0.2 Hz.

B. Microwave-Power Shift Effect

The clock frequency sensitivity to microwave power fluctuations, referred to as microwave-power shift (MPS) [16], arises from the inhomogeneity of the applied microwave field amplitude across the clock cell [22]. The inhomogeneous amplitude distribution of various other fields across the cell results in spatially varying frequency shifts for the Rb atoms effectively localized in the buffer-gas. Hence, the optically detected signal at the end of the cell represents an average of these frequencies [31], [32] weighted by the local microwave field amplitude. Numerical calculations performed for our clock setup allow identifying the highest contribution to the MPS effect as the inhomogeneity of the light shift (LS) caused by the residual coherence [22]. Microwave power fluctuations contribute to the clock instability also through the cavity-pulling effect as discussed in Section III-F.

The measured clock frequency shift is reported in Fig. 4 as a function of the pulse area $\theta = b \cdot T_m \propto \sqrt{P_m}$, for optical pump frequencies tuned to the sub-Doppler peaks from $|5^2S_{1/2},\ F = 2\rangle$ ground state. The pulse area θ and the microwave Rabi frequency b are varied by changing the microwave power P_m, at constant pulse duration T_m. At a microwave pulse area of $\theta = 0.56 \cdot \pi$, slightly larger than the conventional $\theta = \pi/2$ pulses [27] the clock sensitivity to microwave power fluctuations is reduced to $<4 \times 10^{-13}$ /μW. Nevertheless, clock operation with $\theta = 0.56 \cdot \pi$ results in a slightly reduced (by <5%) central fringe contrast and shifts the clock frequency by <25 mHz.

For measuring the microwave power fluctuations in the vapor cell, we make use of the atomic response. For this, we operate the clock with $\theta = 0.8 \cdot \pi$ corresponding to a frequency sensitivity coefficient degraded by one order of magnitude (6×10^{-12} /μW). During the measurement shown in Fig. 5, the clock instability contribution due to intensity light-shift is lower than those from the MPS effect by a factor of 2, and all other effects are at least one order of magnitude lower. Microwave power fluctuations (left axis in Fig. 5) of 1.5×10^{-2} μW (0.08%) at one-day timescale lead to a clock instability contribution (right axis in Fig. 5) $\leq 6 \times 10^{-15}$ when operating at $\theta = 0.56 \cdot \pi$. Furthermore, an active microwave power stabilization scheme, such as the one proposed in [33], benefitting from the pulse interrogation approach and from the atoms' response may be useful to decrease the microwave power fluctuations. In this case, not only the contribution of the MPS effect but also that of the cavity-pulling effect (see Section III-F) via fluctuations of θ would be reduced.

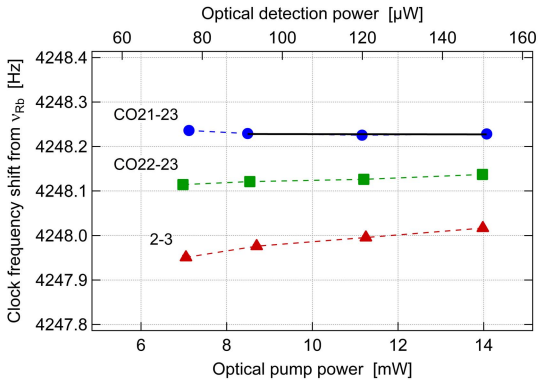

Fig. 6. Clock frequency shift as a function of the optical-pumping pulse power, for laser frequencies labeled, as shown in Fig. 1(c).

C. Light-Shift Effects

Light-induced shifts of the atomic hyperfine splitting frequency, commonly named LSs[1] [34], are a well-known phenomenon in CW-DR and CPT interrogation schemes. When the microwave interrogation takes place in the presence of the laser light, fluctuations of the laser intensity or frequency can, in many of these clocks, present one of the main sources of medium- to long-term clock instability [6], [35], [36]. In the POP interrogation scheme, the optical and microwave interactions are separated in time, which strongly reduces the coupling between the two fields. Yet, the LSs in the POP scheme are not completely eliminated. The remaining clock frequency sensitivity results from a combination of different processes that are associated with each phase of the interrogation scheme: residual coherence due to non-ideal optical pumping in the vapor cell [37], and the residual light during the microwave interrogation due to nonperfect light extinction through the ac Stark shift effect [21].

Fig. 6 reports the clock frequency as a function of the light intensities, varied by the same ratio in all phases of the interrogation scheme, for laser frequency tuned on the sub-Doppler peaks from $|5^2S_{1/2}, F = 2\rangle$ ground state. In the optical power region corresponding to the clock operating conditions (14-mW optical pump power), the clock frequency varies linearly with light intensity. The sensitivity coefficient to light intensity fluctuations, the intensity LS coefficient α_{LS}, is deduced for a fixed laser frequency (black solid line in Fig. 6). As for the sensitivity coefficient to light frequency fluctuations, the frequency LS coefficient β_{LS}, is obtained at a fixed optical power. Table I summarizes the LS coefficients deduced from Fig. 6. Both coefficients are reduced by one order of magnitude compared to the CW-DR [6] and CPT [35] interrogation schemes and are of the same order of magnitude, as the ones reported for similar pulsed DR [9] and CPT schemes [38].

[1]Often the term "light shift" refers to a phenomenological change of clock frequency upon a variation of the light intensity or frequency, while its underlying physical effect is the ac Stark shift [34]. In the POP scheme, other light-induced frequency shifts exist that also depend on the light intensity and frequency, such as, e.g., a residual atomic coherence after the pumping pulse.

TABLE I
INTENSITY AND FREQUENCY LIGHT-SHIFT COEFFICIENTS

	α_{LS}	β_{LS}
CO21-23	$< 2.3 \cdot 10^{-14}$ /%	
CO22-23	$(7\pm2) \cdot 10^{-14}$ /%	$(1.5\pm0.1) \cdot 10^{-13}$ /MHz
2-3	$(1.6\pm0.1) \cdot 10^{-13}$ /%	

Typical optical power fluctuations were measured using the residual transmitted light at the back of a dielectric mirror conducting the light to the clock PP. They are at the level of 0.7% at one-day timescale. For the α_{LS} coefficients listed in Table I, the clock instability contribution from the intensity LS is on the 10^{-14} level. In our clock setup, the laser intensity is not actively stabilized, and its fluctuations represent the main instability source on long-term timescales. Laser intensity fluctuations are affected by the environmental parameters, such as the temperature, pressure, or humidity that may influence via the AOM, optics, and electronics. The laser frequency-stabilization loop may also contribute to the light intensity fluctuations since it acts on the laser current to regulate its frequency. For reducing these long-term instability contributions due to light intensity fluctuations, active laser intensity stabilization is required and can be implemented by, e.g., acting on the laser temperature or via the AOM drive power. Considering that the relative laser intensity fluctuations may be drastically reduced down to the level of 2×10^{-6} at $\tau = 10^4$ s [39] with a stabilization loop via the RF power of the employed AOM, our clock's instability contribution from the intensity LS effect would improve by more than three orders of magnitude to the 5×10^{-18} level. Besides decreasing the laser intensity fluctuations, detailed investigation on the processes contributing to the LSs in the POP scheme, particularly in view of reducing the residual coherence via a stronger optical pumping [37] would help to improve the clock stability limits due to this effect. Moreover, composite interrogation protocols based on the time-domain Ramsey scheme [38] [40] widely exploited to reduce the light-shift effects in recent high-performing CPT-based vapor-cell clock demonstrations may also be an interesting alternative to consider in future studies. Laser frequency fluctuations are measured as 4 kHz at one-day timescale and lead to a clock instability contribution below the 10^{-15} level.

D. Second-Order Zeeman Shift Effect

The clock frequency, insensitive to magnetic field fluctuations in the first order, is impacted by the second-order Zeeman shift [7] according to

$$\Delta\nu_{\mathrm{Zeeman}} = C_2 \cdot B_0^2 \tag{1}$$

where $C_2 = 575.14 \times 10^8$ Hz/T^2 and B_0 is the amplitude of the magnetic field (C-field). From (1), the relative clock frequency sensitivity coefficient to the C-field fluctuations can

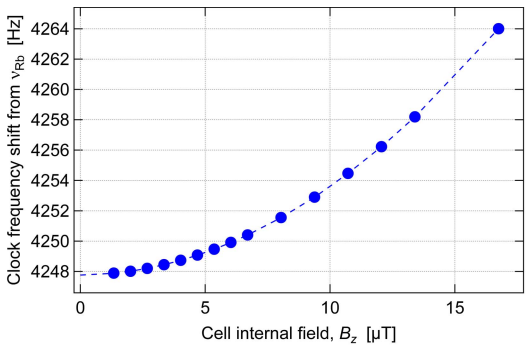

Fig. 7. Clock frequency shift as a function of the applied C-field amplitude.

be written as

$$\frac{\partial \Delta\nu_{\mathrm{Zeeman}}/\nu_{\mathrm{Rb}}}{\partial B_z} = 2 \cdot C_2 \cdot B_0. \qquad (2)$$

The clock frequency shift measured for increased C-field amplitude is shown in Fig. 7. Applying a low C-field of 3.5 μT to the vapor cell leads to a reduced clock frequency sensitivity 5.8×10^{-5}/T and a clock frequency shift of 0.7 Hz.

Once more, we exploit the atomic response to measure the fluctuations of the C-field amplitude in the clock cell. In this case, we measure the frequency fluctuations of the atomic transition $|5^2S_{1/2},\ F = 1,\ m_F = -1\rangle \rightarrow |5^2S_{1/2},\ F = 2,\ m_{F'} = -1\rangle$ that has an increased magnetic field sensitivity $\Delta\nu_{\mathrm{Zeeman}} = C_1 \cdot B_0 + C_2 \cdot B_0^2$ with the linear Zeeman shift coefficient $C_1 = -2 \times 7 \times 10^9$ Hz/T. The measured C-field fluctuations are reported in Fig. 8, together with those of the external magnetic field outside the clock PP (measured with a fluxgate sensor) and the direct current generating the C-field, expressed in terms of magnetic field fluctuations (left axis). The right-hand axis shows the corresponding clock instability contribution. On short-term timescales, magnetic field fluctuations in the clock cell are limited by the noise of the current source. On long-term timescales, field fluctuations in the clock cell are on the level of 20 pT, mainly limited by the external field fluctuations that are attenuated by the magnetic shielding factor ~300 of the PP. The corresponding clock instability contribution is 1.2×10^{-15} at one-day timescale.

E. Buffer-Gas Induced Temperature Coefficients

Temperature fluctuations in the vapor cell impact the clock frequency through the temperature-dependent buffer-gas pressure shift [41] and via buffer-gas density changes in the cell caused by temperature fluctuations of the cell stem [42]. Temperature variations also have an impact on the clock frequency through the spin-exchange effect [43], [44] that is discussed in Section III-G for our clock.

The clock frequency shift induced by the buffer-gas pressure P_{BG} depends on the cell temperature T as

$$\Delta\nu_{\mathrm{BG}} = P_{\mathrm{BG}}\left(\beta + \delta(T - T_0) + \gamma\,(T - T_0)^2\right) \qquad (3)$$

where T_0 is a reference temperature for which the coefficients β, δ, and γ are determined [41]. Thanks to the buffer-gas mixture used in our clock cell, the cell temperature coefficient

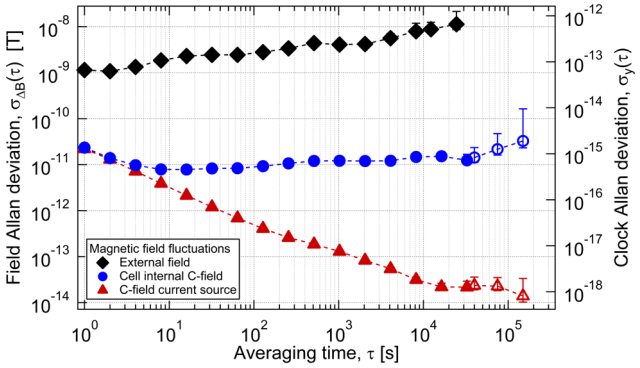

Fig. 8. Magnetic field fluctuations external to the PP for the component parallel to the C-field (diamonds), inside the cell (circles), and the equivalent field fluctuations of the C-field drive current fluctuations (triangles). Left axis: in terms of the magnetic field. Right axis: in terms of relative clock frequency fluctuations.

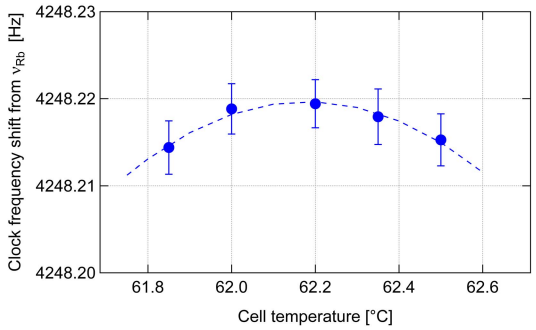

Fig. 9. Clock frequency shift as a function of the cell temperature. Stem temperature is 59 °C.

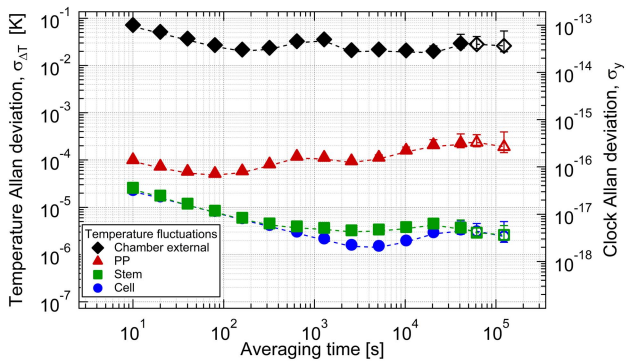

Fig. 10. Temperature fluctuations measured on the cell-cavity assembly (circles) and on the stem (squares) of the clock PP, inside the thermal isolation layers (triangles) on a separate and identical PP in ambient laboratory conditions, and in the laboratory (diamonds). Left axis: in terms of the temperature. Right axis: in terms of relative clock frequency obtained using the stem temperature sensitivity coefficient of 1.3×10^{-12}/K.

is minimized at the so-called inversion point corresponding to a cell temperature of 62.16 °C (cf. Fig. 9) and a frequency sensitivity of $\pm 2.3 \times 10^{-12}$/K in an interval of 0.5 K. The temperature coefficient due to the stem temperature fluctuations in our clock is 1.2×10^{-12}/K.

Temperature fluctuations were measured simultaneously on different locations of the PP, using resistive temperature sensors. Fig. 10 shows the various temperature instabilities: on the cell-cavity assembly and the stem using the PP located

in the chamber, inside the PP thermal isolation layers on a separate and nominally identical PP placed in the ambient laboratory conditions, and in the laboratory. Considering an upper limit for temperature fluctuations of the entire clock cell at the level of 0.5 mK (PP temperature), the estimated clock instability contribution from both—cell and stem—temperature coefficients is at the level of 10^{-15} or below at one-day timescale. The clock frequency shift due to the buffer-gas pressure shift effect at a cell temperature of 62.16 °C is 4248.22 Hz (total buffer-gas pressure of ∼32.5 hPa).

In principle, temperature fluctuations inside the vapor cell can also be assessed by measuring the clock frequency fluctuations using a cell temperature with increased temperature sensitivity. Nevertheless, for temperature fluctuations to become the dominant clock instability source, the cell temperature should be changed by more than ±5 °C which is impractical in our clock, and therefore, was not undertaken.

F. Cavity-Pulling Effect

The clock frequency shift due to the feedback of the microwave cavity with the resonance frequency detuned from the atomic transition by $\Delta\nu_{\rm cav}$ is given by [18]

$$\Delta\nu_{\rm CP} = -\frac{4}{\pi}\frac{Q_L}{Q_a}\Delta\nu_{\rm cav}\ln(\cosh(A)-\mathrm{sgn}(\Delta_i)\cos(\theta)\sinh(A)) \tag{4}$$

where Q_a and Q_L are atomic and loaded cavity quality factors, respectively, Δ_i is the ground-state population inversion at the end of optical pumping pulse ($\Delta_i = -1/3$ in the case of perfect optical pumping as considered here), and $A = \frac{k}{\gamma_2}|\Delta_i|(1-e^{-\gamma_2 T_{\rm Ramsey}})$ with k the microwave photon emission rate by an Rb atom, and γ_2 the ground-state coherence relaxation rate. Q factor and frequency detuning of the magnetron-type cavity measured in the hermetic chamber at 535 hPa are ∼140 and 1.9 MHz, respectively. The measured temperature sensitivity of the cavity resonance frequency is -40×10^3 Hz/K and its pressure and humidity sensitivities, calculated for our microwave cavity according to [30], are -1.6×10^3 Hz/hPa and -37.5×10^3 Hz/(g/m^3), respectively. The clock frequency sensitivity coefficients resulting from cavity pulling and typical parameter fluctuations measured for one-day timescale are resumed in Table II, for our clock under conditions of reduced environmental pressure fluctuations, $\theta = 0.56\cdot\pi$, and optical pumping frequency tuned on a sub-Doppler peak from the $|5^2S_{1/2},\ F=2\rangle$ ground state. We find that clock instabilities due to the cavity-pulling effect are dominated by the humidity sensitivity of the cavity and the microwave power fluctuations, which leads to a clock instability contribution one order of magnitude lower than the MPS effect. The other instability contributions via the cavity-pulling effect are at negligible levels, also when considering the ambient laboratory conditions.

G. Spin-Exchange Effect

The spin-exchange frequency shift due to the collisions between Rb atoms is given by [43], [44]

$$\Delta\nu_{\rm SE} = -\frac{1}{8\pi}n\bar{v}\lambda_{\rm SE}\langle\Delta\rangle_{T_{\rm Ramsey}} \tag{5}$$

TABLE II

CLOCK SENSITIVITY COEFFICIENTS AND ESTIMATED CLOCK INSTABILITY CONTRIBUTIONS DUE TO THE CAVITY-PULLING EFFECT

for $10^4<\tau<10^5$s	*Sensitivity coefficient*	*Parameter fluctuations*	*Clock instability*
Temperature	$-5.1\cdot10^{-15}$ /K	$<5\cdot10^{-4}$ K	$<2.6\cdot10^{-18}$
Pressure	$-2\cdot10^{-16}$ /hPa	$<3\cdot10^{-2}$ hPa	$<6\cdot10^{-18}$
Humidity	$-4.8\cdot10^{-15}$ /(g/m^3)	<0.4 g/m^3	$<1.9\cdot10^{-15}$
Microwave power	$5.6\cdot10^{-14}$ /μW	$<1.5\cdot10^{-2}$ μW	$<8.3\cdot10^{-16}$
Total contribution			$<2.1\cdot10^{-15}$

where n is the Rb atomic density, $\bar{v}$ is the average relative velocity of two colliding atoms, $\lambda_{\rm SE}$ is the spin-exchange cross section, and $\langle\Delta\rangle_{T_{\rm Ramsey}}$ is the average population difference between the two hyperfine ground states during the Ramsey time. The change of the Rb density in the vapor cell that contributes to the clock signal is of the order of 9% for a temperature change of 1 K. The fluctuations of the temperature result in a spin-exchange induced clock frequency sensitivity of 6×10^{-12}/K. Temperature fluctuations <0.5 mK at one-day timescale (cf. Section III-E) contribute to the clock instability via the spin-exchange effect at a level of 3×10^{-15}.

IV. LONG-TERM INSTABILITY BUDGET

Table III summarizes the physical effects impacting the long-term frequency stability of our vapor-cell clock with experimentally measured sensitivity coefficients and parameter fluctuations under the clock-operation conditions. Experimentally, the measured sensitivity coefficients of the barometric and MPS effects and the temperature coefficients include the impacts of cavity-pulling and spin-exchange effects; therefore, in Table III, only the dominant effects are indicated. The estimated clock instability contributions are given for averaging times from 10^4 to 10^5 s (one day) under typical laboratory conditions and result in a total clock instability of 1.7×10^{-14}, in good agreement with the measured stability shown in Fig. 2(b). We estimate other effects, such as the blackbody radiation shift [45], the direct current Stark shift [46], and frequency shifts due to helium permeation through the glass cell walls [47] to contribute to the clock instability at one-day timescale at the level of 10^{-15} or well below.

The long-term clock stability was optimized by selecting proper experimental parameters. The instability contributions from the MPS and second-order Zeeman shift effects were reduced by optimizing the microwave pulse area and C-field amplitude. The change of the pulse area from $\pi/2$ to $0.56\cdot\pi$ implies a small compromise on the clock frequency shift and slightly reduced contrast of the central Ramsey fringe (by less than 5%) but results in an improvement of long-term clock stability by about one order of magnitude. The contributions from the frequency light-shift and buffer-gas shift temperature coefficients remain at the level of 10^{-15} or below, as well as the ones from cavity-pulling and spin-exchange effects.

TABLE III

LONG-TERM CLOCK INSTABILITY BUDGET FOR $10^4 < \tau < 10^5$ S. FOR THE SENSITIVITY COEFFICIENTS AND THE PARAMETER FLUCTUATIONS, THE UPPER LIMITS ARE GIVEN, THUS THE CLOCK INSTABILITY CONTRIBUTIONS REPRESENT THE ESTIMATIONS FOR MAXIMAL CONTRIBUTIONS

Physical effect	*Relative sensitivity coefficient*	*Parameter fluctuation* σ_p *(*$10^4 < \tau < 10^5$ *s)*	*Clock instability contribution* σ_y *(*$10^4 < \tau < 10^5$ *s)*
Barometric [a]	$6.6\cdot10^{-14}$ /hPa	$3\cdot10^{-2}$ hPa	$2.0\cdot10^{-15}$
Microwave-power shift [a]	$4.0\cdot10^{-13}$ /μW	$1.5\cdot10^{-2}$ μW	$6.0\cdot10^{-15}$
Intensity light shift	$2.3\cdot10^{-14}$ /%	0.7 %	$1.6\cdot10^{-14}$
Frequency light shift	$1.5\cdot10^{-13}$ /MHz	$4\cdot10^{-3}$ MHz	$6.0\cdot10^{-16}$
Second-order Zeeman shift	$5.8\cdot10^{-5}$ /T	$2\cdot10^{-11}$ T	$1.2\cdot10^{-15}$
Buffer-gas shift – Stem TC [b]	$1.2\cdot10^{-12}$ /K	$5\cdot10^{-4}$ K	$6.0\cdot10^{-16}$
Buffer-gas shift – Cell TC [a,b]	$2.3\cdot10^{-12}$ /K	$5\cdot10^{-4}$ K	$1.2\cdot10^{-15}$
Total clock instability, $[\sum_i \sigma_i^2]^{1/2}$			$1.7\cdot10^{-14}$

[a] Including the cavity-pulling effect contribution
[b] Including the spin-exchange effect contribution

Compared to previous measurements, the contribution from the barometric effect is strongly reduced thanks to the hermetic chamber. This operation mode allows analyzing the achievable stability performance of our clock under conditions of reduced barometric effect, such as when operated in a vacuum or with a vapor cell with reduced barometric sensitivity. The dominant clock instability contribution then arises from the laser intensity fluctuations. We, therefore, also suspect the observed bump in Fig. 2(b) around 10^4 s to arise from this effect. An active stabilization loop acting through the laser temperature or the AOM that reduces the laser intensity fluctuations at the PP input by a factor of 3 will be sufficient for reaching a $<10^{-14}$ clock stability level at one day timescale. Alternatively, detailed analyses on the light-induced clock frequency sensitivities in pulsed DR schemes would help to identify the physical processes at the origin of this dominant contribution.

V. CONCLUSION

We reported on our analyses of the long-term instability sources at the level of $\leq 10^{-14}$ in a compact Rb vapor-cell clock based on a time-domain Ramsey interrogation scheme with pulsed optical pumping and detection, in view of a highly compact atomic clock operating under ambient laboratory conditions with a strongly simplified PP. We evaluated the long-term stability limitations at one-day timescale arising from various instability contributions due to typical experimental and environmental parameter fluctuations. The overall clock stability limit estimated from the measured parameter fluctuations agrees well with the measured long-term clock instability of $<2 \times 10^{-14}$ at one-day timescale and is dominantly limited by laser intensity fluctuations. This clock stability limit can still be considerably improved by the implementation of an active laser intensity stabilization loop or possibly by further investigations to quantify and reduce the impact of different physical processes of the intensity light-shift in the POP scheme (e.g., stronger optical pumping to reduce the residual coherence). While in the present study, we employed a hermetic chamber to demonstrate the clock performance at 10^{-14} level under reduced barometric effect, similar results are expected from a new vapor-cell design (in terms of cell geometry and/or buffer-gas mixture [23]) with a barometric sensitivity reduced by two orders of magnitude. Finally, such improvements are expected to allow the development of a compact and high-performance vapor-cell clock with a simplified PP, without need for a vacuum enclosure.

ACKNOWLEDGMENT

The authors would like to thank M. Pellaton and S. Kang (both previously LTF) for their previous work, and M. Durrenberger and P. Scherler (both LTF) for their technical support. They would also like to thank C. Calosso (INRIM) for the microwave synthesizer, A. Landragin (Observatoire de Paris) for helpful discussions, and A. Jallageas (METAS) for the fluxgate sensor, and MeteoSuisse, the Swiss Federal Office of Meteorology and Climatology, for providing the environmental data.

Experimental results presented in this work are open-access available under DOI: http://doi.org/10.23728/b2share.6c52dbf74afd422c9587ff71cf9bdd99.

REFERENCES

[1] L. Maleki and J. Prestage, "Applications of clocks and frequency standards: From the routine to tests of fundamental models," *Metrologia*, vol. 42, pp. S145–S153, Jun. 2005.

[2] L. A. Mallette, "Atomic and quartz clock hardware for communication and navigation satellites," in *Proc. 39th Annu. Precise Time Time Interval (PTTI) Meeting*, 2007, pp. 1–15.

[3] M. Lévesque and D. Tipper, "A survey of clock synchronization over packet-switched networks," *IEEE Commun. Surveys Tuts.*, vol. 18, no. 4, pp. 2926–2947, 4th Quart., 2016.

[4] L. Zhan, Y. Liu, W. Yao, J. Zhao, and Y. Liu, "Utilization of chip-scale atomic clock for synchrophasor measurements," *IEEE Trans. Power Del.*, vol. 31, no. 5, pp. 2299–2300, Oct. 2016.

[5] J. G. Fletcher, M. Chaluvadi, D. M. Anand, J. Amelot, Y. Li-Baboud, and J. Moyne, "Smart clocks have a hand in the smart grid," in *Proc. IEEE Power Energy Soc. Gen. Meeting*, Jul. 2011, pp. 1–6.

[6] T. Bandi, C. Affolderbach, C. Stefanucci, F. Merli, A. K. Skrivervik, and G. Mileti, "Compact, high-performance CW double-resonance rubidium standard with $1.4\times10^{-13}\tau^{-1/2}$ stability," *IEEE Trans. Ultrason., Ferroelectr., Freq. Control*, vol. 61, no. 11, pp. 1769–1778, Nov. 2014.

[7] J. Vanier and C. Mandache, "The passive optically pumped Rb frequency standard: The laser approach," *Appl. Phys. B, Lasers Opt.*, vol. 87, no. 4, pp. 565–593, 2007.

[8] J. Camparo, "The rubidium atomic clock and basic research," *Phys. Today*, vol. 60, no. 11, pp. 33–39, 2007.

[9] S. Micalizio, C. E. Calosso, A. Godone, and F. Levi, "Metrological characterization of the pulsed Rb clock with optical detection," *Metrologia*, vol. 49, no. 4, p. 425, 2012.

[10] S. Kang, M. Gharavipour, C. Affolderbach, F. Gruet, and G. Mileti, "Demonstration of a high-performance pulsed optically pumped Rb clock based on a compact magnetron-type microwave cavity," *J. Appl. Phys.*, vol. 117, no. 10, 2015, Art. no. 104510.

[11] Q. Hao, W. Li, S. He, J. Lv, P. Wang, and G. Mei, "A physics package for rubidium atomic frequency standard with a short-term stability of $2.4\times10^{-13}\tau^{-1/2}$," *Rev. Sci. Instrum.*, vol. 87, Dec. 2016, Art. no. 123111.

[12] G. Dong, J. Deng, J. Lin, S. Zhang, H. Lin, and Y. Wang, "Recent improvements on the pulsed optically pumped rubidium clock at SIOM," *Chin. Opt. Lett.*, vol. 15, no. 4, p. 040201, 2017.

[13] J. Vanier, "Atomic clocks based on coherent population trapping: A review," *Appl. Phys. B, Lasers Opt.*, vol. 81, no. 4, pp. 421–442, 2005.

[14] F. Levi, A. Godone, and J. Vanier, "The light shift effect in the coherent population trapping cesium maser," *IEEE Trans. Ultrason., Ferroelectr., Freq. Control*, vol. 47, no. 2, pp. 466–470, Mar. 2000.

[15] T. Zanon, S. Guérandel, E. de Clercq, D. Holleville, N. Dimarcq, and A. Clairon, "High contrast Ramsey fringes with coherent-population-trapping pulses in a double lambda atomic system," *Phys. Rev. Lett.*, vol. 94, no. 19, 2005, Art. no. 193002.

[16] W. J. Riley, Jr., "The physics of the environmental sensitivity of rubidium gas cell atomic frequency standards," *IEEE Trans. Ultrason., Ferroelectr., Freq. Control*, vol. 39, no. 2, pp. 232–240, Mar. 1992.

[17] S. Micalizio, A. Godone, F. Levi, and C. Calosso, "Medium-long term frequency stability of pulsed vapor cell clocks," *IEEE Trans. Ultrason., Ferroelectr., Freq. Control*, vol. 57, no. 7, pp. 1524–1534, Jul. 2010.

[18] A. Godone, S. Micalizio, F. Levi, and C. Calosso, "Physics characterization and frequency stability of the pulsed rubidium maser," *Phys. Rev. A, Gen. Phys.*, vol. 74, no. 4, p. 043401, 2006.

[19] N. Almat, M. Gharavipour, W. Moreno, C. Affolderbach, and G. Mileti, "Long-term stability analysis towards <10–14 level for a highly compact POP Rb cell atomic clock," in *Proc. Joint Conf. IEEE Int. Freq. Control Symp. Eur. Freq. Time Forum (IEEE IFCS-EFTF)*, 2019, Paper 0063.

[20] C. Stefanucci *et al.*, "Compact microwave cavity for high performance rubidium frequency standards," *Rev. Sci. Instrum.*, vol. 83, no. 10, 2012, Art. no. 104706.

[21] M. Gharavipour *et al.*, "High performance vapour-cell frequency standards," *J. Phys., Conf. Ser.*, vol. 723, no. 1, 2016, Art. no. 012006.

[22] W. Moreno *et al.*, "Impact of microwave-field inhomogeneity in an alkali vapour cell using Ramsey double-resonance spectroscopy," *Quantum Electron.*, vol. 49, pp. 293–297, Mar. 2019.

[23] W. Moreno, M. Pellaton, C. Affolderbach, and G. Mileti, "Barometric effect in vapor-cell atomic clocks," *IEEE Trans. Ultrason., Ferroelectr., Freq. Control*, vol. 65, no. 8, pp. 1500–1503, Aug. 2018.

[24] C. E. Calosso, S. Micalizio, A. Godone, E. K. Bertacco, and F. Levi, "Electronics for the pulsed rubidium clock: Design and characterization," *IEEE Trans. Ultrason., Ferroelectr., Freq. Control*, vol. 54, no. 9, pp. 1731–1740, Sep. 2007.

[25] S. Kang, M. Gharavipour, F. Gruet, C. Affolderbach, and G. Mileti, "Compact and high-performance Rb clock based on pulsed optical pumping for industrial application," in *Proc. Joint Conf. IEEE Int. Freq. Control Symp. Eur. Freq. Time Forum*, Apr. 2015, pp. 800–803.

[26] S. Micalizio, A. Godone, C. Calosso, F. Levi, C. Affolderbach, and F. Gruet, "Pulsed optically pumped rubidium clock with high frequency-stability performance," *IEEE Trans. Ultrason., Ferroelectr., Freq. Control*, vol. 59, no. 3, pp. 457–462, Mar. 2012.

[27] C. Affolderbach *et al.*, "Selected studies on high performance laser-pumped rubidium atomic clocks," in *Proc. IEEE Int. Freq. Control Symp. (IFCS)*, May 2018, pp. 1–6.

[28] G. Iyanu, H. Wang, and J. Camparo, "Pressure sensitivity of the vapor-cell atomic clock," *IEEE Trans. Ultrason., Ferroelectr., Freq. Control*, vol. 56, no. 6, pp. 1139–1144, Jun. 2009.

[29] M. Huang, C. M. Klimcak, and J. C. Camparo, "Vapor-cell clock frequency and environmental pressure: Resonance-cell volume changes," in *Proc. IEEE Int. Freq. Control Symp.*, Jun. 2010, pp. 208–211.

[30] A. Godone, S. Micalizio, F. Levi, and C. Calosso, "Microwave cavities for vapor cell frequency standards," *Rev. Sci. Instrum.*, vol. 82, pp. 074703-1–074703-15, Jul. 2011.

[31] A. Risley, S. Jarvis, Jr., and J. Vanier, "The dependence of frequency upon microwave power of wall-coated and buffer-gas-filled gas cell Rb^{87} frequency standards," *J. Appl. Phys.*, vol. 51, pp. 4571–4576, Sep. 1980.

[32] G. Mileti, I. Ruedi, and H. Schweda, "Line inhomogeneity effects and power shift in miniaturized rubidium frequency standards" in *Proc. EFTF*, Jun. 1992, pp. 515–519.

[33] M. Gozzelino, S. Micalizio, F. Levi, A. Godone, and C. E. Calosso, "Reducing cavity-pulling shift in Ramsey-operated compact clocks," *IEEE Trans. Ultrason., Ferroelectr., Freq. Control*, vol. 65, no. 7, pp. 1294–1301, Apr. 2018.

[34] B. S. Mathur, H. Tang, and W. Happer, "Light shifts in the alkali atoms," *Phys. Rev.*, vol. 171, no. 1, pp. 11–19, Jul. 1968.

[35] M. A. Hafiz, G. Coget, P. Yun, S. Guérandel, E. de Clercq, and R. Boudot, "A high-performance Raman-Ramsey Cs vapor cell atomic clock," *J. Appl. Phys.*, vol. 121, no. 10, 2017, Art. no. 104903.

[36] P. Yun *et al.*, "High-performance coherent population trapping clock with polarization modulation," *Phys. Rev. Appl.*, vol. 7, no. 1, 2017, Art. no. 014018.

[37] A. Godone, S. Micalizio, and F. Levi, "Pulsed optically pumped frequency standard," *Phys. Rev. A, Gen. Phys.*, vol. 70, no. 2, Aug. 2004, Art. no. 023409.

[38] M. A. Hafiz *et al.*, "Symmetric autobalanced Ramsey interrogation for high-performance coherent-population-trapping vapor-cell atomic clock," *Appl. Phys. Lett.*, vol. 112, no. 24, 2018, Art. no. 244102.

[39] F. Tricot, D. H. Phung, M. Lours, S. Guérandel, and E. Clercq, "Power stabilization of a diode laser with an acousto-optic modulator," *Rev. Sci. Instrum.*, vol. 89, no. 11, 2018, Art. no. 113112.

[40] M. Shuker *et al.*, "Ramsey spectroscopy with displaced frequency jumps," *Phys. Rev. Lett.*, vol. 122, no. 11, 2019, Art. no. 113601.

[41] J. Vanier, R. Kunski, N. Cyr, J. Y. Savard, and M. Têtu, "On hyperfine frequency shifts caused by buffer gases: Application to the optically pumped passive rubidium frequency standard," *J. Appl. Phys.*, vol. 53, no. 8, pp. 5387–5391, 1982.

[42] C. E. Calosso, A. Godone, F. Levi, and S. Micalizio, "Enhanced temperature sensitivity in vapor-cell frequency standards," *IEEE Trans. Ultrason., Ferroelectr., Freq. Control*, vol. 59, no. 12, pp. 2646–2654, Dec. 2012.

[43] S. Micalizio, A. Godone, F. Levi, and J. Vanier, "Spin-exchange frequency shift in alkali-metal-vapor cell frequency standards," *Phys. Rev. A, Gen. Phys.*, vol. 73, no. 3, Mar. 2006, Art. no. 033414.

[44] S. Micalizio, A. Godone, F. Levi, and J. Vanier, "Erratum: Spin-exchange frequency shift in alkali-metal-vapor cell frequency standards [Phys. Rev. A 73, 033414 (2006)]," *Phys. Rev. A, Gen. Phys.*, vol. 74, no. 5, Nov. 2006, Art. no. 059905.

[45] E. J. Angstmann, V. A. Dzuba, and V. V. Flambaum, "Frequency shift of hyperfine transitions due to blackbody radiation," *Phys. Rev. A, Gen. Phys.*, vol. 74, no. 2, Aug. 2006, Art. no. 023405.

[46] J. R. Mowat, "Stark effect in alkali-metal ground-state hyperfine structure," *Phys. Rev. A, Gen. Phys.*, vol. 5, no. 3, pp. 1059–1062, Mar. 1972.

[47] S. Abdullah, C. Affolderbach, F. Gruet, and G. Mileti, "Aging studies on micro-fabricated alkali buffer-gas cells for miniature atomic clocks," *Appl. Phys. Lett.*, vol. 106, Apr. 2015, Art. no. 163505.

Nil Almat received the M.S. degree in micro-engineering from École Polytechnique Fédérale de Lausanne, Lausanne, Switzerland, in 2014. She is currently pursuing the Ph.D. degree in physics with Laboratoire Temps-Fréquence, Université de Neuchâtel, Neuchâtel, Switzerland.

In 2015, she worked as a Research and Development Engineer at Alpes Lasers SA, St. Blaise, Switzerland. In 2016, she joined the Laboratoire Temps-Fréquence, University of Neuchâtel. Her research interests include atomic spectroscopy, stabilized lasers, and vapor-cell frequency standards.

Mohammadreza Gharavipour received the M.S. degree in advanced materials (nanotechnology) from the University of Ulm, Ulm, Germany, in 2011, and the Ph.D. degree in physics from the University of Neuchâtel, Neuchâtel, Switzerland, in 2018.

From 2011 to 2013, he worked as a Process Engineer with OptoGaN GmbH, Landshut, Germany. He is currently a Process Engineer with TRUMPF Photonic Components (Registered Legal Entity: Philips Photonics GmbH), Ulm.

William Moreno received the M.S. degree in physics from École Polytechnique Fédérale de Lausanne (EPFL), Lausanne, Switzerland, in 2014, and the Ph.D. degree in physics from Neuchâtel University, Neuchâtel, Switzerland, in 2019.

He is currently a Postdoctoral Researcher at Laboratoire national de métrologie et d'essais, Système de Références Temps-Espace (LNE-SYRTE), Paris, France. His research interests include atomic spectroscopy, quantum physics, stabilized lasers, and frequency standards.

Florian Gruet received the Dipl.Ing. degree in microtechnics from the Specialized Engineer School (HES-SO), Le Locle, Switzerland, in 2008.

In 2008, he joined Laboratoire Temps-Fréquence, Université de Neuchâtel, Neuchâtel, Switzerland, as a Scientific Collaborator. His research interests include optical systems and stabilized lasers.

Christoph Affolderbach (M'13) received the Diploma and Ph.D. degrees in physics from Bonn University, Bonn, Germany, in 1999 and 2002, respectively.

From 2001 to 2006, he was a Research Scientist at Observatoire Cantonal de Neuchâtel, Neuchâtel, Switzerland. In 2007, he joined Laboratoire Temps-Fréquence, Université de Neuchâtel, Neuchâtel, where he is currently working as a Senior Scientific Collaborator. His research interests include the development of stabilized diode laser systems, atomic spectroscopy, and vapor-cell atomic frequency standards, in particular, laser-pumped high-performance atomic clocks, and miniaturized frequency standards.

Gaetano Mileti (M'12) received the Diploma degree in physics from École Polytechnique Fédérale de Lausanne, Lausanne, Switzerland, in 1990, and the Ph.D. degree in physics from the University of Neuchâtel, Neuchâtel, Switzerland, in 1995.

From 1991 to 1995 and from 1997 to 2006, he was a Research Scientist at Observatoire Cantonal de Neuchâtel, Neuchâtel. From 1995 to 1997, he was at the National Institute of Standards and Technology, Boulder, CO, USA. In 2007, he co-founded Laboratoire Temps—Fréquence (LTF), Université de Neuchâtel, where he is currently the Deputy Director and an Associate Professor. His research interests include atomic spectroscopy, stabilized lasers, and frequency standards.